Design and Production of Magnetic Environment Simulation Equipment for MIST

Carl Järmyr Eriksson and Valentin Minoz

***Abstract*—This report describes the design and production of a 3-axis Helmholtz coil assembly and its control unit. The purpose of the system is to simulate the magnetic environment that the CubeSat MIST will need to measure in order to determine and control its attitude. To achieve this, the system consists of three Helmholtz coils with diameters of roughly 1 metre, supplied by a circuit that filters, transforms, and amplifies signals of 0-5 V (e.g. Arduino signals) to -50 to 50 V. The size of the coils allow for a near-homogeneous magnetic field large enough to cover the whole satellite. By adjusting the input, two necessary tests can be done on the satellite's attitude determination and control system. The first consists of verifying the magnetometer's correct measurement of the direction of the ambient magnetic field, and the other of testing the detumbling capability of the system when the satellite is in a rotating field. The equipment produced has been tested to verify its operation meets set requirements for testing.**

***Index Terms*—MIST, microsatellite, ADCS, magnetometer, Helmholtz coil, Arduino.**

I. Introduction

The project consists of producing a 3-axis coil system for testing the on-board magnetometer of the MIST satellite, a 3U CubeSat under development at KTH since early 2015 [1]. The system consists of 3 superposed Helmholtz coils, independently controlled, to produce a variable field in any direction. Helmholtz coils consist of a pair of identical coils in series separated by the same distance as their radii, producing a volume of quasi-uniform magnetic field when subject to a current [2]. Similar systems have previously been used for developing and testing attitude determination systems similar to the aforementioned satellite's, e.g. by [3].

Once deployed in orbit, the attitude of the satellite is controlled by its Attitude Determination and Control System (ADCS). The ADCS uses a combination of sun sensors and magnetometers in order to determine the orientation of the satellite, and a set of magnetorquers which can produce a magnetic dipole in order to control the orientation of the satellite. This configuration is common for microsatellites [4].

Controlling the attitude and orientation of the satellite is mission critical. It is required for the on-board experiments and solar panels, in addition to detumbling the satellite once it is released from the launch vehicle. Therefore, testing the components of the ADCS prior to flight is key to the success of the MIST project.

II. Project Aim

Several uses for a magnetic field simulator have been considered: testing the magnetometers of the satellite; testing the magnetic properties of the satellite or its components; evaluating the magnetorquers and their detumbling capability. While all of these functions are desirable, achieving all of them was deemed difficult given the time and resources available. Therefore, the aim of this project is to produce a magnetic field generator to test the magnetometers.

The system should simulate the expected magnetic field in orbit that the magnetometers are to measure, for both static and rotating fields.

III. Method / Design process

This section details the process involved in producing the magnetic field simulator system.

A. System Requirements

The aim of the project imposes a set of requirements for the system's design, listed below:

1) **Homogeneous magnetic field with strength of 130 μT.**
   In order to simulate the Earth's magnetic field in orbit, the system must be able to cancel out the Earth's ambient magnetic field at the location of testing, then generate a sufficiently strong field in any direction. In other words, the maximum field strength which the system should produce is two times that of the Earth's magnetic field. Earth's field has a maximum of $\sim 65\ \mu T$ at surface [5]. Since the orbit of MIST is low (640km, an order of magnitude smaller than Earth's radius), the magnetic field strength is not significantly weaker than at surface. In addition, the produced field must be as homogeneous as possible, in direction and strength, to properly cancel the ambient field and mimic the expected field.
2) **Generated fields should be well-defined.**
   In order to assess any tests properly, the generated fields need to be well-defined. Therefore the construction of the coils and the method for varying the field need to be accurate.
3) **Whole satellite should fit inside.**
   If one wants to be able to test the magnetic properties of the satellite itself, and their possible effect on the magnetometer, the produced field must be of appropriate volume. Since the satellite has a volume of $10 \times 10 \times 30$ cm^3, the field needs to be 30 cm wide in each direction.
4) **Ability to rotate field.**
   Rotating the field is necessary to recreate a rotation of the satellite, experienced for example during its detumbling phase. The expected speed of rotation is up

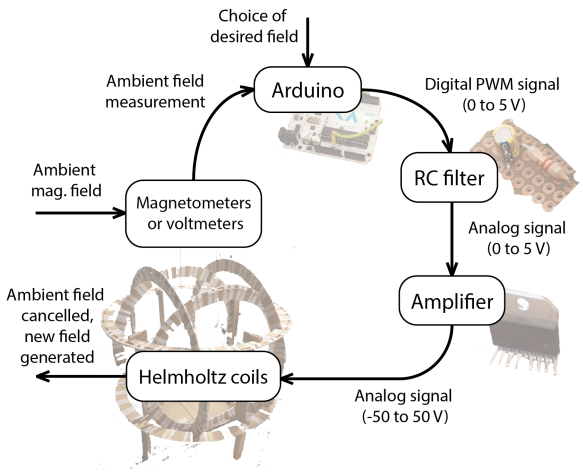

Fig. 1. Schematic design of the magnetic field simulator system.

to 20°/s (18 seconds period) [6], the ADCS must as such be tested for similar and reasonably faster (up to at least 40°/s is desireable) rotations of the field the satellite is under.

B. Overview

Given these requirements, a plan for the system was made. It can be summarized as follows, with the help of Fig. 1: the ambient magnetic field is measured; an Arduino provides three pulse width modulated (PWM) signals based on the ambient field and the desired field to be applied. RC filters convert the PWM signals to analog, which are then amplified by high power amplifiers. The amplified voltages are applied on three Helmholtz coils (one per cartesian axis), producing the desired field whilst cancelling the ambient field. The specifics of this design and corresponding reasoning is described in the subsections below.

C. Dimensions

Due to the size of Earth's magnetic field, the MIST satellite will at any given point in time experience a homogeneous field both in terms of direction and field strength. This can be achieved with part of the field generated by a Helmholtz coil.

Helmholtz coils consist of two identical coils separated from each other at a distance equal to their equal radii, with the equal currents passing through, as shown in Fig. 2.

The relationship between the current passed through the coils and the generated magnetic field is given by the Biot-Savart law [7]:

$$\mathbf{B}(\mathbf{r}) = \frac{\mu_0}{4\pi}\int \frac{\mathbf{I}\times\hat{\mathbf{r}}'}{r'^2}dl', \tag{1}$$

where $\mathbf{B}(\mathbf{r})$ denotes the magnetic field vector at a given point, I the current, $\hat{\mathbf{r}}'$ the unit displacement vector from the wire element dl' to $\mathbf{r}$, r' the length of that displacement vector, and μ_0 the permeability of free space. Using this equation, the magnetic field created by a Helmholtz coil was simulated in MATLAB.

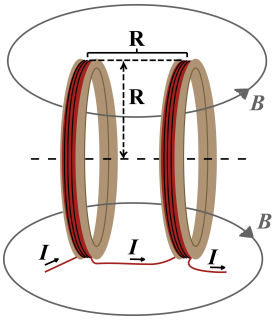

Fig. 2. Simplified view of a Helmholtz coil. R denotes the radius, which is equal the distance between the two coils. A current I is passed through the coils producing a magnetic field $\mathbf{B}$. The image, and notably the shape of $\mathbf{B}$, not to scale.

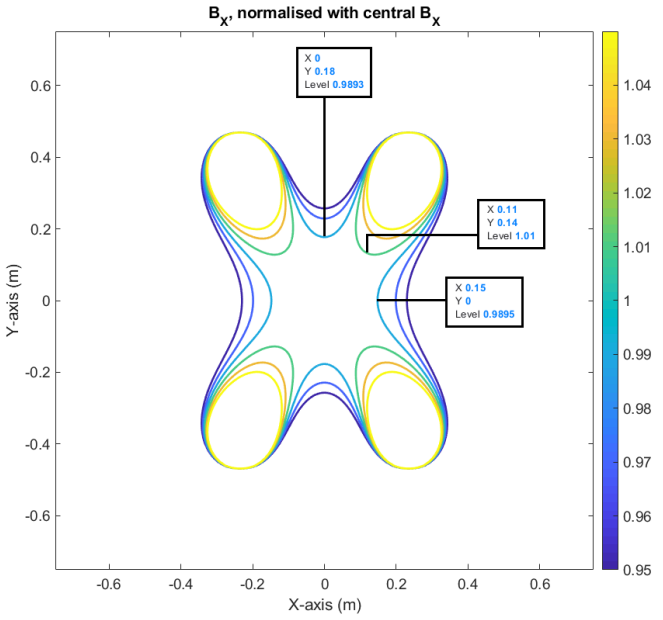

Fig. 3. Relative magnetic field strength in X-direction. The graph is a cross-section of the magnetic field along the coils' axis of symmetry. The smallest distance from the origin to the 1% level curve is 15 cm.

The field generated by a Helmholtz coil is most homogeneous in a volume surrounding the midpoint in between the two coils. Considering firstly the field strength, the tolerance for field strength homogeneity was decided to be within $\pm 1\%$ of the midpoint's field strength. Under this condition, a Helmholtz coil with arbitrary radius R has a cylindrical volume of (by our tolerance) homogeneous field strength roughly $\frac{2}{3}R$ wide and of similar diameter. This can be seen in Fig. 3, which shows the field strength of a cross-section of the field created by a Helmholtz coil with $R = 50$ cm.

Homogeneity in field direction could be defined as the Y- and Z- components of the field having a field strength of 0, provided that the X-direction is along the coil's line of symmetry. The volume where the Y- and Z- components are less than $\pm 1\%$ of the midpoint's field strength (in X-direction) is slightly larger than the aforementioned volume of field strength homogeneity; as visible in Fig. 4. Therefore, $\frac{2}{3}R$ is the limiting dimension of the effective field; a coil radius of

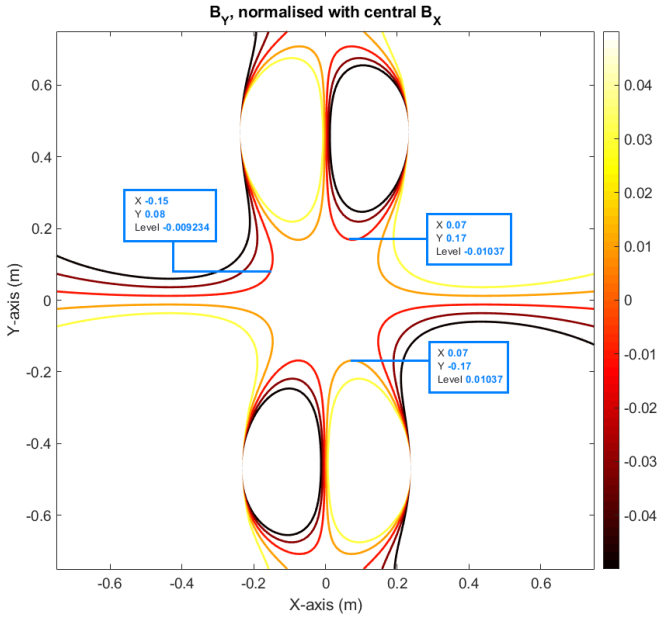

Fig. 4. Magnetic field strength relative to central B_X in Y-direction. The graph is a cross-section of the magnetic field along the coils' axis of symmetry; the field strength in Z-direction is the same due to symmetry. The smallest distance from the origin to the 1% level curve is 17 cm.

50 cm gives the volume of the field with 1% difference from the midpoint field a smallest width of around 30 cm, enough to envelop the entire satellite. Thus, every Helmholtz coil to be used in the system must be roughly this size or larger in order to fulfill Requirement 3.

Given a coil radius of 50 cm, an appropriate current, number of turns, and wire type must be determined to attain the desired field strength (Requirement 1). The Biot-Savart law can be applied to get the field produced by a circular loop carrying a steady current I. This gives the following, with x being the distance from center along the coil's line of symmetry,

$$B(x) = \frac{\mu_0}{2\pi}\frac{R^2}{(R^2+x^2)^{3/2}}. \tag{2}$$

The field is only in the x-direction. For a Helmholtz coil the field along this axis is a superposition of the fields of the two coils composing it. Taking into account the number of turns, N, of the coil, the total field strength can be expressed as

$$B(x) = \frac{N\mu_0 R^2}{2\pi}\Big(\frac{1}{(R^2+(x-\frac{R}{2})^2)^{3/2}} + \frac{1}{(R^2+(x+\frac{R}{2})^2)^{3/2}}\Big) \tag{3}$$

Given the radius $R = 50\ cm$, the field $B(x=0)$ must reach 130 μT (Requirement 1), where $x = 0$ is the midpoint on the coil's axis of symmetry and corresponds to the midpoint in Figures 3 and 4. A balance between current, wire thickness and number of turns in each coil pair must be decided. A series of relationships must be considered for these parameters,

$$B(0)\propto I,\ B(0)\propto N,\ B(0)\propto\frac{1}{R},\ I\propto\frac{1}{N},\ N\propto R. \tag{4}$$

The relationship between $B(0)$, $N \cdot I$ is given by a factor

$$K = \frac{\mu_0 R^2}{(R^2+\frac{R}{2}^2)^{3/2}} = \frac{B(x)}{NI}. \tag{5}$$

As a consequence of these relationships, a 2 A current along approximately 37 turns of 0.5 mm diameter enamelled wire delivers the maximum field strength for each coil pair. A stronger current would be more difficult to provide for all three coils while requiring thicker, more expensive wires. A lower current would require more turns, unfeasible given the wiring on all six coils was to be done by two persons. The chosen current gives a number of turns suitable for the conditions at hand (economic, time, manpower, etc.), with the appropriate wire type. The wire itself ('*DASOL - Round enamelled winding wire of copper, solderable, class 155*' [8]) has a cross sectional area of 0.2 mm^2, which can safely carry 2 A, with good heat tolerance for prolonged use. Additionally, copper of 0.2 mm^2 has a resistance per metre of 0.08545 Ω/m, for a total of approx. 20 Ω for each coil pair in series. This requires a high voltage to get 2 A along a coil pair (45 V $\Longrightarrow$ 90 W).

D. Coil Assembly

With coil radii around 50 cm, the three coil pairs would require a cubic metre of space once assembled. For this reason, it was decided to make the supporting structure easy to disassemble. Consequently, all six coils have separate supporting rings. Furthermore, in order to superpose the axes of each coil pair, the radii of the different coil pairs and their rings cannot be the same. The radii for the coil pairs for directions X, Y and Z are 47, 51 and 54 cm respectively, adjusted such that the ratio R/N is constant. Given the parameters previously set, this sets the appropriate numbers of turns to 34, 37 and 39 respectively (33.98, 36.87 and 39.04; rounded to nearest integer). As such, the field produced per current applied remains constant.

The material used for the supporting rings is masonite board. The material is light and slightly elastic which makes the rings easily handled during assembly. However, the material is less sturdy and requires more careful handling than e.g. wood. To hold the wiring of the coils, creating a fully circular support was not deemed possible. Instead a triacontagonal (30-sided polygon) support was designed, with 30 wooden dowels inserted into the masonite rings, around which the wires are coiled. Although a triacontagon differs from a circle, the differences are negligible; the decrease in circumference is $\sim 0.2\%$ and the minimum radius is $\sim 0.5\%$ smaller than the maximum radius. Finally, with the coils wired around the dowels, masking tape is used to secure the coils to the rings. This was used as it was readily available, is easily applied in large quantities and is easy to remove if need be.

To give the overall structure rigidity, the horizontal coil pair stands on 6 legs, and braces keep them at the correct distance apart. Each ring pair has notches at the intersections with the smaller ring pair, such that a fit with correct distancing is made with ease every time the structure is assembled.

The resulting assembly and its magnetic properties are presented in Section IV-A.

E. Control Unit Design

To produce an arbitrary static field, one can manually provide appropriate currents to each separate coil, following the measurements in Section IV, or by comparing to a calibrated magnetometer. However, producing rotating fields to accurately mimic rotation in space, requires a proper control unit. It must apply 3 separate, slowly changing DC currents (periods of 18 seconds and slower won't be found in low-frequency AC supplies) with controllable amplitudes, phases and period. Given the resistance of the coils, the amplitude of the voltage supplied must be upwards of 45 V. Using a low pass filter, PWM signals from an Arduino can provide the control needed, however an Arduino can only supply 5 V. The design of the circuit is therefore based on using high power audio amplifiers to amplify the waves. This is what determined the main system structure, presented in Section III-B.

In order to supply up to 50 V in both directions smoothly, three LM4766 [9], which incorporate two high power audio amplifiers each, were used. These amplifiers are designed to continuously output 30 W per channel on average, whereas the system will require a maximum of approximately 90 W. Therefore, the amplifiers are mounted on a large aluminium heat sink, the LM4766 are notably not robust at temperatures higher than 150°C [9]. Audio amplifiers were chosen for their fidelity in giving an output signal with the same characteristics as the input, as opposed to e.g. motor drivers, which are not designed to give a smooth output voltage. For example: Full-Bridge Motor Driver LMD18245T delivers current in steps [10] .

The circuitry and its design process are described in the following two sections, *Intended Circuitry* and *Final Circuitry*, with associated diagrams in Figures 5 and 6.

1) Intended Circuitry: Fig. 5 is circuit diagram for the originally intended control system. The principle is that the positive voltages are applied by the amplifier to the left (U1), and the negative by the right (U2). The filtered (by RC filter) signal, between 0 and 5 V, is the non-inverting input (+) of U1. The amplifier amplifies the signal by 10.2, since the amplification is given by $\frac{R1+(R2+R_v)}{R1}$ in this configuration. By itself this gives the ability to supply 0 to 50 V to any coil with its other end at ground, however, the system must be able to provide -50 to 50 V. Therefore, U2 is set up to invert the output of U1 with half of the supplied voltage as a reference. If U1 outputs 0 V, U2 will give -50 V on the coil, similarly 25 V gives -25 V, for a net 0 V. One can express this, ideally, as

$$\begin{aligned} V_{coil} &= V_{OutU1} - V_{OutU2} \\ &= V_{OutU1} - (2 \cdot \text{Half}V_{CC} - V_{OutU1}) \\ &= 20.4 \cdot V_{input} - 50 \end{aligned} \tag{6}$$

The power supply for the system consists of two parallel voltage supplies set to 25 V, in series so that 25 V (HalfV_{CC}) can be taken over one and 50 V (V_{CC}) over both. There is an issue with this setup, in that the input that gives 0 V on the coils can change and must be determined experimentally, since it depends on how well the power supply is configured and on the amplification (see eq. (6)). Ideally the '+' input of U2 (HalfV_{CC}) is exactly half of V_{CC}, such that the system can provide as much negative voltage as positive. To find the input that outputs 0 V, a feedback system (in the green-bounded area of Fig. 5) consisting of voltage dividers provides small voltages back to the microcontroller to read from analog ports. A calibration program can be written for the microcontroller to sweep through all PWM duty ratio levels to find the one that gives the closest difference in voltage to 0.

This system was simulated through transient analysis on TINA-ti, a SPICE-based circuit simulator program that Texas Instruments distributes [11]. The model for LM4766 is available from Texas Instruments, that manufactures the component, and the simulated circuit as described and shown on Fig. 5 functioned as desired. In reality however, there is a condition stated in the data sheet that the V_{EE} of the component must be 9 V below the GND, whereas the circuit was intended to have the same ground as V_{EE} for the amplifiers. The circuit therefore does not work with the LM4766, and adjustments are necessary.

2) Final Circuitry: The power supply is not shown in Fig. 6, it is similar to that in Fig. 5, but with each voltage supply set to 30 V rather than 25 V, for additional margin. The relative ground is set to be between the two supplies, such that 30 V, 0 V, and -30 V are provided through the bus on the lower edge of the diagram. This results in 60 V between V_{EE} and V_{CC} on the amplifiers, which is still within what LM4766 is designed for [9]. This system has V_{EE} and GND now separated by 30 V, and the second amplifier, now denoted 'B' having 0 V as + input. The main difference compared to the intended system is that the dual amplifier configuration no longer translates low, positive voltage inputs to negative outputs; 0 V input relative to GND gives 0 V output. To rectify this, low power operational amplifiers, AD822 [12], were set up to bring down the input by 2.5 V. The AD822 are added after the filtering of the signal, act as inverters, similarly to the B amplifiers, with 1.25 V as reference (+ input). The relationship between output voltage and input voltage can be summarised similarly to eq. (6) as

$$\begin{aligned} V_{coil} &= V_{OutA} - V_{OutB} \\ &= V_{OutA} - (-V_{OutA}) \\ &= 2 \cdot 10.2 \cdot V_{OutAD822} \\ &= 20.4 \cdot (V_{input} - 2 \cdot 1.25) \\ &= 20.4 \cdot V_{input} - 51. \end{aligned} \tag{7}$$

The circuits are practically equivalent, but the final system requires more components, since three additional voltages must be supplied to the added op-amp. 1.25 V was chosen to give a 0 V output in the middle of the 0-5 V range of the signal, and the amplifier is itself supplied with 15 V and -12 V. The latter voltages were used because AD822 can take up to $\pm 15V$ [12] and L78S15CV and LM7912 regulators were available. A potentiometer, RV was used to take approx. 1.25 V from the 15 V provided by the L78S15CV.

The issue with 0 V output not necessarily being exact

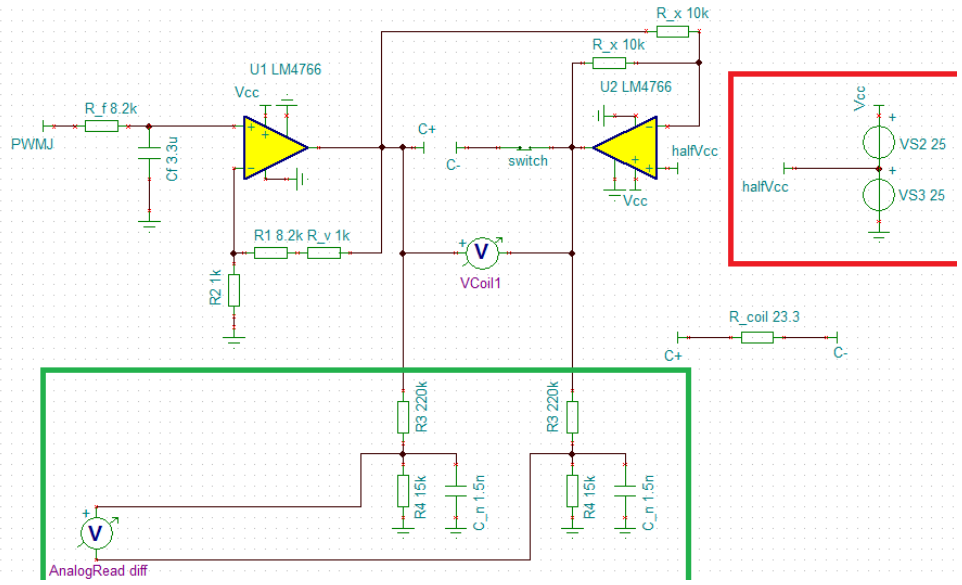

Fig. 5. Circuit diagram produced in TINA-ti. The input PWM signal relative to ground enters through PWMJ in the upper left. The region bounded by red is the power supply and by green is the proposed feedback system.

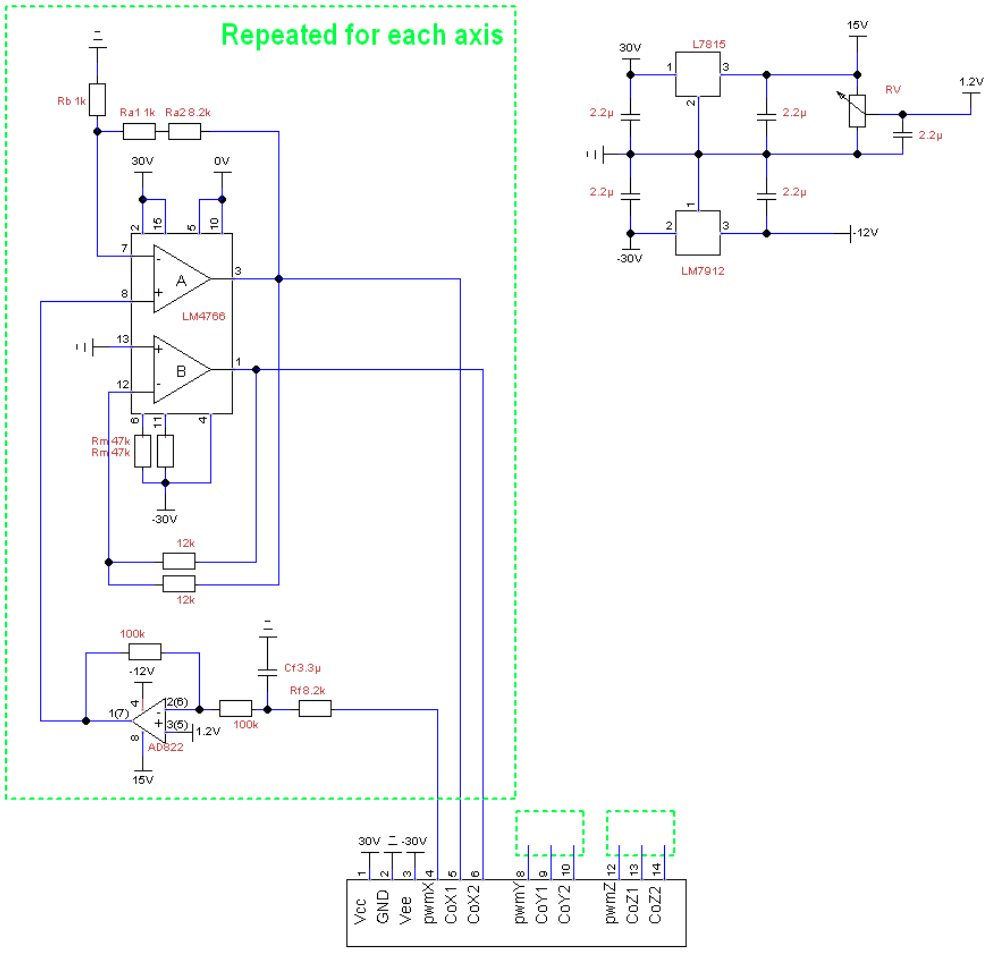

Fig. 6. Circuit diagram produced in TinyCAD. This reflects the final circuit made. The large green dash-bounded region is repeated for each axis; the small similarly bounded areas represent identical circuits. Rm disables the mute function as prescribed by the LM4766 data sheet [9]. The diagram depicts the board as used, so external components are not included. The power supply is connected to bus ports 1-3, the Arduino to 4, 8 and 12.

Fig. 7. The three-axis Helmholtz coil assembly, the smallest coil pair defines the X-axis, the intermediate Y, and the largest, horizontal pair is Z.

remains, but due to time limitations, the feedback system in Fig. 5 was not implemented in the final circuit. However, since the associated input to output 0 V is largely based on the + voltage of the AD822, in turn given by the setting of the potentiometer, the latter was adjusted to match a 0 V output as close as possible to 2.47 V in input (equivalent to duty ratio level 126 from the microcontroller).

F. Software

In order to provide the PWM signal to the circuit, two Arduino programs are written; *staticfield.ino* and *rotating-field.ino*, shown in Appendix A. The programs convert desired input values in μT to PWM duty ratio levels for the microcontroller's PWM output, based on measured properties presented in the results Section IV.

IV. Results

A. Helmholtz Coil Assembly

The magnetic field produced by the the coil assembly was tested using magnetometers. First of all, the relationship between current and magnetic field strength was determined for each axis. This was done using both a flux-gate magnetometer and a smartphone magnetometer. The flux-gate magnetometer is accurate to less than 0.2 μT [13] and the smartphone's accuracy is unknown prior to the measurements. The results are shown in Fig. 8.

The resulting gradients for the field strength-to-current relationships for each axis were: 65.48 μT/A for X; 66.14 μT/A for Y; 65.43 μT/A for Z. Fig. 8 shows the measurements, with very similar field strength-current relationships for all axes. This suggests that the adjustments in number of turns in the coils, described in Section III-D, worked as intended.

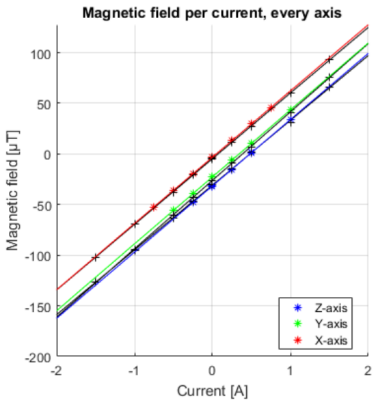

Fig. 8. The magnetic field strength as a function of current supplied, for each axis. The coloured data is from the flux-gate magnetometer and the black data is from the smartphone magnetometer.

The vertical offset is the ambient field in which the measurements were made. This experiment also served to compare the smartphone magnetometer (black data) to the flux-gate (coloured data). It was deduced that the smartphones were accurate enough to be used for testing, the lowest observed accuracy being ± 2.5 μT. Due to availability limitations and a sufficient accuracy measured for the smartphone magnetometer, all subsequent magnetic field measurements are made with the smartphone.

The homogeneity of the near-homogeneous area of the field was also tested. The smartphone magnetometers were used to measure the field strength in each direction at 27 discrete points within a volume $30 \times 30 \times 30$ cm^3 around the midpoint. For each point two measurements were taken, measuring firstly the ambient field and secondly the ambient field plus a generated static field. Fig. 9 shows the points in space and the measured total field strength minus the total ambient field for each point. The corner points, which were the furthest from the midpoint, experienced the largest deviations from the midpoint field with 1 A applied, in all directions. This is shown in Table I. The results suggest that the field

	Mean difference from midpoint (%) when running 1 A		
Axis	Side points	Edge points	Corner points
X	1.17	2.64	7.11
Y	0.84	1.94	3.61
Z	1.31	1.07	3.89

TABLE I
THE (PERCENTUAL) MEAN DIFFERENCE BETWEEN THE MIDPOINT FIELD STRENGTH (APPROX. 65 μT) AND THE FIELD STRENGTHS FOR THE SIDE POINTS; EDGE POINTS; CORNER POINTS.

is largely homogeneous; the side and edge points are within the volume of near-homogeneity discussed in III-C and have small average deviations from the midpoint field strength. The corner points are outside of this volume and are thus expected to deviate more.

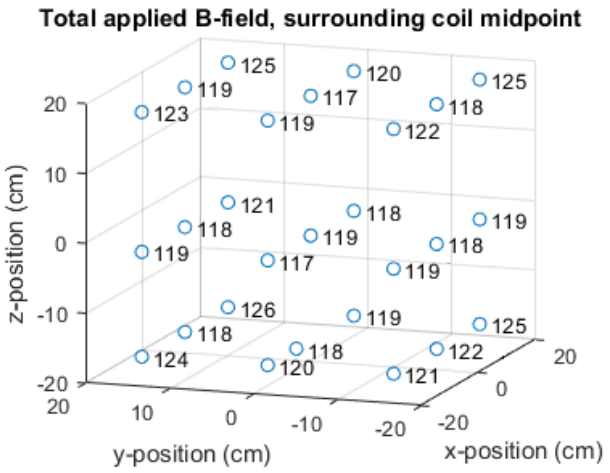

Fig. 9. Total generated field (in μT) for each position of points tested. The midpoint of the coil assembly is the origin for the coordinates. Error estimated to ± 4 μT.

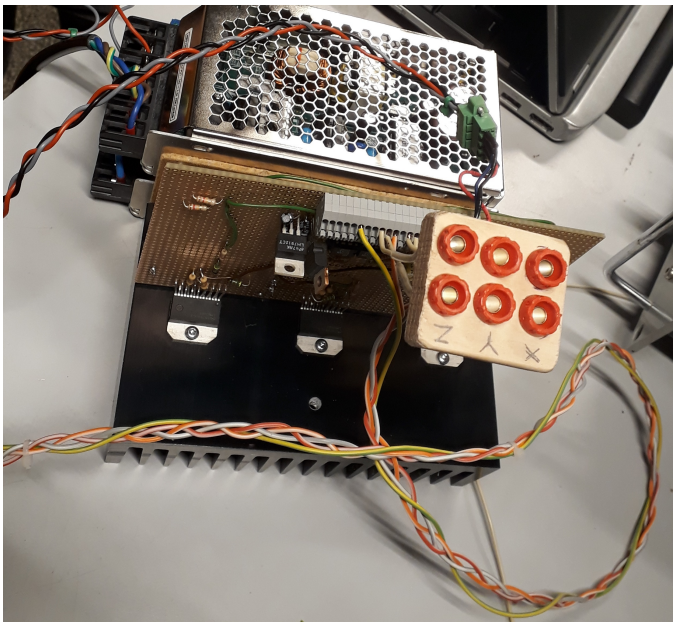

Fig. 10. The circuit, with banana sockets for connecting the coils and the power supply behind it. The long 4-wire braid goes to the microcontroller to carry the three PWM signals and GND.

B. Control system

By using the data in Section IV-A and the measured resistance of the coil pairs, a voltage-magnetic field strength relationship was assumed, since the voltage is what can be controlled using the circuit made. Further converting to V_{input} (by measured outputs for different inputs) and Arduino PWM duty ratio levels (from 0 to 255, equivalent to 0 to 5 V), a V_{in}/μT and level (lv) per μT relationship is assumed. These relationships are presented along with the radius, number of turns, and resistance for each coil pair in Table II.

The transformation from PWM to analog signals with the RC filters in the circuitry is simple but entails some noise, as it is not a perfect low pass filter. The RC filter used (R $=$ 8.2 $k\Omega$, C $=$ 3.3 μF) was set by testing different values for

Axis	R (m)	N	res (Ω)	μT/A	V/μT	V_{in}/μT	lv/μT
X	0.47	34	17.8	65.48	0.27	0.015	0.76
Y	0.51	37	20.9	66.14	0.32	0.017	0.887
Z	0.54	39	23.3	65.43	0.36	0.02	0.996

TABLE II
PROPERTIES OF EACH COIL PAIR. NOTE: THE V_{in} TO V_{out} GRADIENT IS APPROX. 18.2 WITH THE CIRCUIT, WITH 0 OUTPUT FOR $\sim$2.47 V INPUT.

Fig. 11. Sine wave produced using *rotatingfield.ino* on the circuit (yellow), and the frequency distribution calculated by the FFT function on an oscilloscope (pink).

the resistance and capacitance to have a fast enough response time but as little noise as possible. The RC time constant $\tau = (3.3\ \mu \cdot 8.2\ k)$s gives it a cutoff frequency of $f_c = \frac{1}{2\pi\tau} = 5.88$ Hz. Fig. 11 shows the output of the circuit when sending a signal using *rotatingfield.ino*. The filtered and amplified sine wave retains some of the original signal as noise, as can be seen with FFT analysis, the main peak is the 1/4 Hz desired sine wave, but at 500 Hz a second peak, though much weaker, matches the Arduino's PWM frequency [14]. That 'residue' of the original signal can be seen in the output wave as noise, but it's amplitude is, as suggested by the FFT graph, relatively low. It is worth noting that these results were measured with the circuit not being connected to the coils, as their impedance might help reduce the high frequency noise. This is discussed further in the next section.

With the three major components of the system combined; the Arduino, circuitry and coil assembly, the system requirements of Section III-A are met to a satisfactory level. The process of applying an arbitrary field is fairly simple, step by step:

1) Set up the coil assembly as in Fig. 7.
2) Connect the coil pairs together with their respective blade connectors, then to the appropriate circuit outputs using 4mm banana connectors.
3) Connect the circuit to the power supply as shown in Fig. 10, but wait before connecting it to mains electricity.
4) Connect the PWM inputs to respective Arduino pins and the Arduino to a computer.
5) Set the *staticfield.ino* program to apply no field; 0 μT in all directions, and send it to the microcontroller.

6) Measure the ambient field in the coil assembly. Power the power supply; if the field changes by more than the accuracy desired, adjust the baseline values in the program and try again until this is no longer the case.
7) Now that correct baselines are set, set the ambient field strength values in the program to the measured field, and the desired field to e.g. 30 μT. If the magnetic field is not as close to **B** = (30, 30, 30) μT as desired, adjust the lv/μT values until it is.
8) Now that the correct baselines and ratios are found, the system is calibrated for its current arrangement. To apply an arbitrary static or rotating field, use the appropriate program with these values and designate the ambient and desired field strengths (as well as period and phases for rotation).

Steps 5 through 7 are to calibrate the system for its current properties, which not a time consuming process, with the values from Table II as starting points. This will be discussed further in Section V-C.

V. Discussion

A. Accuracy of the Coil Assembly

The accuracy of the coils is vital to the functionality of the whole system. If the coils and the supporting structure vary too much from the theoretical design, the generated fields could differ from expectations and affect the 'well defined' requirement.

For the field homogeneity tests, most of the points tested are outside of the theoretically near-homogeneous volume, as the lower coil radii of the X and Y axes means a smaller $\frac{2}{3}R$. Despite this, the deviations from the midpoint field strength are sufficiently low in most of the points measured; the corner points experience higher deviations but are outside of the near-homogeneous volume. Furthermore, it is very possible that a lot of the variations in the data was caused by inaccuracy of the magnetometer used. Ideally one would want a more accurate magnetometer and more data points to accurately map the homogeneity of the field; difficulties with positioning the magnetometer correctly and the overall inaccuracy of the magnetometer used made extensive testing redundant.

The disassemblability of the coil structure also limits its accuracy. To make assembling easy the number of external struts and connections between the coil pairs is kept at a minimum, and the notches at the intersections between the rings are the main way of positioning the coils at appropriate distances. If the structure was permanent, it would allow for greater control of the inaccuracies from the geometry. Since the rings themselves were sawed manually their diameters vary slightly in some places (~ 0.5 cm). This could mean that the contact points with other rings differ from the theoretical design, altering the positions of the coils slightly. Apart from this, the assembly looks satisfactory with the naked eye; the coils in each respective pair are parallel and have the correct distances from each other.

B. Filtering and Noise

When measuring the output with an oscilloscope (for Fig. 11), a simple resistor was used in place of a coil. This is due to no oscilloscope being available where the coils are stored at the time of writing this report. It may or may not have an effect on the result, and may be investigated in future work, but assuming it does not, it would be preferable to attenuate the 500 Hz residue further. Lowering the cutoff frequency of the existing RC filter by increasing either the capacitance or resistance would increase the response time too much, so changing to a second order filter is a better option. Considering that low power op amps (AD822) are already in place, one could construct an active second order filter for each input channel using them, which would enable stronger attenuation of high frequencies for the same response time. Although this would increase the complexity of the circuitry, it may be considered if the noise proves to be a problem in the future.

C. Calibration

In part due to the use of banana connectors between the coil assembly and circuitry, the resistance on which the amplified voltage is applied varies, and since the current is what determines the field strength produced, the lv/μT ratio is not necessarily constant between two uses of the system. The baselines, inputs for which the outputs are 0 V, may also change, as mentioned with the design process of the circuitry. As such, the calibration steps in Section IV-B should be followed before each use. If the circuitry was designed to regulate current instead of directly amplifying voltage, this would not be necessary; though such an electrical system would have to be more complex.

To instead automate the calibration of the software, two changes to the system can be made:

1) A calibrated magnetometer can be used by the Arduino. For example HMC588L, with a possible resolution of 5 μT when calibrated [15], could be on a probe directly connected to the Arduino to feed magnetic field measurements directly to the microcontroller. With a separate calibration program that finds the correct baselines and level-per-μT ratios.
2) To find the correct baselines, an analog feedback, as suggested in the intended circuitry (shown in Fig. 5), could be added, to function as described in the associated Section (III-E1).

D. System and Project Complexity

The initially intended amplifying circuitry was simpler than what was finally constructed, the latter requiring additional op-amps and regulators in order to adjust for the LM4766, as described in Sections III-E1 and III-E2. It is interesting to note that although the initial circuit worked according to TINA-ti, it did not in practice; conversely, the final system does not work in simulation but works well in reality. This serves to highlight the limitations of such simulation software. The adjustments made to the circuit may have made the system more complex than it needed to be, and other overlooked arrangements for providing the high voltage may be better; for exampple, some circuit regulating current based on a voltage input, as was done by Daniel Strufaldi Batista et. al. in [3]. Besides, the issue of

providing high voltage would not be present if the coils were smaller. For example, if at the stage of setting the system requirements, it were decided that only $10 \times 10 \times 10$ cm^3 of near homogeneous field is enough (i.e. fitting the ADCS unit of the satellite), considerably smaller dimensions would entail significantly less power needed. The system that was finally produced is however, as discussed, enough to meet the requirements as set to a satisfying extent, and the ADCS system can be tested with the whole satellite within the coil assembly.

E. Future work

Apart from the previously discussed points of potential improvements to the system, the equipment is to be used for intended purpose; testing the satellite's magnetometer.

The accuracy of the system as a whole could be improved. As mentioned previously, further testing would be required to investigate the homogeneity of the field properly. Accurately determining this would mean a much better accuracy for the system as a whole. Further improvements to the accuracy of the system could involve adding additional structural support to ensure a more precise placement of the rings, and by filtering out noise in the signal as discussed previously.

The software for the control unit could also be built upon. Although the system is capable of producing fields with properties similar to those which the satellite will experience in flight, the existing scripts do not allow for more complex simulations. To simulate a specific scenario, i.e. a certain behaviour of the satellite, the software would require more advanced functions. Combining this with a feedback system such as the one discussed previously, the magnetorquers could potentially be tested by measuring the magnetic dipole moment generated and adjusting the coils' field appropriately.

The satellite's correct measurement of magnetic fields in orbit can now be studied by applying a known field and confirming that the ADCS board sends the correct signals to the on-board computer. The input to the magnetorquers is to be compared to the attitude determined, and their applied dipoles for that input will be verified to be in the right direction.

VI. Conclusion

The system produced is capable of (to some extent) quantitative testing of the satellite's magnetometer with a field mimicking the expected environment well. All of the Requirements 1-4 were achieved, either completely or to a satisfactory extent; the system can immerse the satellite completely in near-homogeneous field, that can be static, rotate, or move in another way, with very simple Arduino code or even a function generator. The overall aim of the project was reached. The system meets the set requirements, although more can be done in the future to optimize the process of using it, along with adding functionalities building on the existing system.

Appendix A – Arduino Code

Acknowledgments

The authors would like to thank their supervisor, Francesca Capel for her guidance, support and kindness throughout the project. They would also like to thank Sven Grahn, for his inspirational leadership of the MIST project and the opportunity to take part in such an exciting endeavor. In addition, they extend their gratitude to Stefan Jacob for providing space to work and store equipment, while providing advice and assistance.

References

[1] A. Gärdebåck. (2019, 2) The student satellite MIST. [Online]. Available: https://www.kth.se/en/sci/centra/rymdcenter/studentsatellit/studentsatelliten-mist-1.481707

[2] R. K. Cacak and J. R. Craig, "Magnetic field uniformity around nearhelmholtz coil configurations," *Review of Scientific Instruments*, vol. 40, no. 11, pp. 1468–1470, 1969. [Online]. Available: https://doi.org/10.1063/1.1683829

[3] D. Strufaldi Batista, F. Granziera, M. Carvalho Tosin, and L. F. de Melo, "Three-axial helmholtz coil design and validation for aerospace applications," *IEEE Transactions on Aerospace and Electronic Systems*, vol. 54, no. 1, pp. 392–403, 2018.

[4] W. H. Steyn and H. W. Jordaan, "An active attitude control system for a drag sail satellite," *Acta Astronautica*, vol. 128, pp. 313–321, 2016.

[5] E. Thébault, C. C. Finlay, C. D. Beggan, P. Alken, J. Aubert, O. Barrois, F. Bertrand, T. Bondar, A. Boness, L. Brocco, E. Canet, A. Chambodut, A. Chulliat, P. Coïsson, F. Civet, A. Du, A. Fournier, I. Fratter, N. Gillet, B. Hamilton, M. Hamoudi, G. Hulot, T. Jager, M. Korte, W. Kuang, X. Lalanne, B. Langlais, J.-M. Léger, V. Lesur, F. J. Lowes, S. Macmillan, M. Mandea, C. Manoj, S. Maus, N. Olsen, V. Petrov, V. Ridley, M. Rother, T. J. Sabaka, D. Saturnino, R. Schachtschneider, O. Sirol, A. Tangborn, A. Thomson, L. Tøffner-Clausen, P. Vigneron, I. Wardinski, and T. Zvereva, "International geomagnetic reference field: the 12th generation," *Earth, Planets and Space*, vol. 67, no. 1, p. 79, May 2015. [Online]. Available: https://doi.org/10.1186/s40623-015-0228-9

[6] S. Chandrashekar, "De-tumbling Analysis of MIST Satellite," Feb. 2016.

[7] D. J. Griffiths, *Introduction to electrodynamics*, 4th ed. University Printing House, Cambridge CB2 8BS, UK: Cambridge University Press, 2017.

[8] Dahrénträd, "Dasol," 2011, certified according to ISO 9001:2000. [Online]. Available: https://www.elfa.se/Web/Downloads/he/et/dasol_eng_datasheet.pdf

[9] National Semiconductor, "Lm4766 overture audio power amplifier series dual 40w audio power amplifier with mute," 2006. [Online]. Available: https://www.elfa.se/Web/Downloads/_t/ds/lm4766_eng_tds.pdf

[10] Texas Instruments, "Lmd18245 3a, 55v dmos full-bridge motor driver," 2013. [Online]. Available: http://www.ti.com/lit/ds/symlink/lmd18245.pdf

[11] ——. (2018) Spice-based analog simulation program - (active) tina-ti. [Online]. Available: http://www.ti.com/tool/TINA-TI

[12] Analog Devices, "Single-supply, rail-to-rail low power fet-input op amp," 2015. [Online]. Available: https://www.analog.com/media/en/technical-documentation/data-sheets/AD822.pdf

[13] LEMI Sensors. (2016, Feb.) Lemi-011. [Online]. Available: https://www.lemisensors.com/?p=133

[14] T. Hirzel. (2019, Apr.) PWM. Arduino.cc's tutorial on pwm. [Online]. Available: https://www.arduino.cc/en/Tutorial/PWM

[15] Honeywell, "3-axis digital compass ic hmc5883l," 2011. [Online]. Available: https://cdn.sparkfun.com/datasheets/Sensors/Magneto/HMC5883L-FDS.pdf